Reduction Behavior of Panzhihua Titanomagnetite Concentrates with Coal

TU HU, XUEWEI LV, CHENGUANG BAI, ZHIGANG LUN, and GUIBAO QIU

The reduction behavior of the Panzhihua titanomagnetite concentrates (PTC) briquette with coal was investigated by temperature-programmed heating under argon atmosphere in a vertical tube electric furnace. The mass loss behavior of the PTC-coal mixture was checked by thermogravimetric analysis method in argon with a heating rate of 5 K (5 °C)/ min. It was found that there are five stages during the carbothermic reduction process of the PTC. The devolatilization of coal occurred in the first stage, and reductions of iron oxides mainly occurred in the second and third stages. The reduction rate of iron oxide in the third stage was much higher than that in the second stage because of the significant rate of carbon gasification reaction. The iron in the ilmenite was reduced in the fourth stage. In the final stage, the rutile was partially reduced to lower valence oxides. The phase transformation of the briquette reduced at different temperatures was investigated by X-ray diffraction (XRD). The main phases of sample reduced at 1173 K (900 °C) are metallic iron, ilmenite ($FeTiO_3$), and titanomagnetite ($Fe_{3-x}Ti_xO_4$). The traces of rutile (TiO_2) were observed at 1273 K (1000 °C). The iron carbide (Fe_3C) and ferrous-pseudobrookite ($FeTi_2O_5$) appeared at 1473 K (1200 °C). The titanium carbide was found in the sample reduced at 1623 K (1350 °C). The shrinkages of reduced briquettes, which increased with increase in the temperature, were found to depend greatly on the temperature. With increasing the reduction temperature to 1573 K (1300 °C), the iron nuggets were observed outside of the samples reduced. The nugget formation can indicate a new process of ironmaking with titanomagnetite similar to ITmk3 (Ironmaking Technology Mark 3).

DOI: 10.1007/s11663-012-9783-7

I. INTRODUCTION

MAGNETITE of Panzhihua, China, is a complex iron ore, containing elements of vanadium and titanium. It accounts for more than 90 pct of the titanium reserves in China.[1] By the beneficiation process of the ore, titanomagnetite concentrates and ilmenite concentrates are produced. The mineralogy of titanomagnetite concentrates has been studied extensively by geologists.[2,3] It consists of titanomagnetite in majority, with less magnetite and ilmenite. Titanomagnetite has a cubic spinel structure. The general formula can be written as AB_2O_4, where A is in tetrahedral coordination and B is in an octahedral site.[4,5] Titanomagnetite ($Fe_{3-x}Ti_xO_4$) is a solid-solution of magnetite (Fe_3O_4) and ulvospinel (Fe_2TiO_4) in which Fe^{3+} in the B sub-lattice of magnetite are replaced by Ti^{4+}, with the concurrent conversion of Fe^{3+} to Fe^{2+} to maintain charge balance.[6]

Most of the titanomagnetite concentrates are used as the main materials for the blast furnace process in Panzhihua area now. Most of the iron and partly of vanadium can be reduced into the hot metal. However, almost all of the titanium still remains in the slag, forming the high-titanium slag in which the content of TiO_2 varies from 22 pct to 25 pct.[1,3,7,8] There is no appropriate and economic method so far to deal with the slag.[3,7,8] In recent years, most of the studies focus on developing an alternative route to use the titanomagnetite concentrates. One potential choice is the rotary hearth furnace process, which involves the reduction step of composite briquette of titanomagnetite concentrates with noncoking coal and the smelting of the reduced sample in an electric-arc furnace.

Direct reduction of titanomagnetite has been widely studied for many decades. It was found that the reduction of titanomagnetite is slower than that of magnetite because of the existence of titanium cations, resulting in a higher thermodynamic stability of titanomagnetite.[1,9–11] Desheng Chen *et al.*[1] studied the effect of preoxidation on the carbothermic reduction of titanomagnetite concentrates by isothermal experiments at 1273 K to 1473 K (1000 °C to 1200 °C) in nitrogen. It was found that the preoxidation processing accelerated the reduction rate of titanomagnetite concentrates due to the destruction of the crystal lattice of raw titanomagnetite concentrates and the formation of pore in the particles. Roshchin *et al.*[12] investigated the solid-state reduction of titanomagnetite concentrates with milled graphite electrodes as the reductant at temperature range 1273 K to 1773 K (1000 °C to 1500 °C). It was found that the metallic iron began to form at the temperature range 1353 K to 1383 K (1080 °C to 1110 °C) and the reduction of titanium oxides began at above 1488 K (1215 °C). Park

TU HU, Ph.D. Student, XUEWEI LV and GUIBAO QIU, Associate Professors, CHENGUANG BAI, Professor, and ZHIGANG LUN, Postgraduate, are with the School of Materials Science and Engineering, Chongqing University, Chongqing 400044, P.R. China. Contact e-mail: lvxuewei@163.com
Manuscript submitted June 15, 2012.
Article published online January 15, 2013.

and Ostrovski[4] studied the reduction of titanomagnetites by nonisothermal and isothermal experiments using CO-CO_2-Ar gas mixtures from room temperature to 1373 K (1100 °C). It was observed that the reduction of titanomagnetites in nonisothermal reduction experiments started at 1073 K (800 °C) and completed at 1373 K (1100 °C). Titanomagnetites were reduced to metallic iron and titanium oxides in 60 minutes in the isothermal reduction at 1373 K (1100 °C) using 75 vol pct CO – 25 vol pct Ar gas mixture. It was suggested that the slowest step was the reduction of titanomagnetite to wustite. Wustite was transformed to metallic iron quite quickly.

Many works can be found in the literature, which are related to reduction in composites of iron oxides and carbon.[13–15] It was established that the reduction proceeds along the sequence $Fe_2O_3 \rightarrow Fe_3O_4 \rightarrow FeO \rightarrow Fe$. The reduction of wustite to metallic iron was found to be the slowest step during the reduction process. It was substantiated that the overall reduction rate for composites was controlled by gasification reaction rate at lower temperature. Fruehan[13] observed that the overall reduction rate deviated from the carbon gasification-controlled regime at a higher temperature. Srinivasan and Lahiri[16] found the rate-controlling reaction could change from carbon gasification to wustite reduction according to the CO_2/CO ratio in the product gas, deending on the amount of carbon in the composites. Some authors[17–20] stated that heat transfer is equally important along with the chemical kinetics of the carbon gasification reaction.

Carbothermic reduction of ilmenite has been investigated by many authors.[21–24] It was found that the carbothermic reduction of ilmenite concentrates strongly depends on temperature, gas composition, and concentrate grade. Welham and Williams[24] investigated the carbothermic reduction of ilmenite and rutile at temperatures up to 1773 K (1500 °C). The reaction was found to proceed *via* an initial, rapid reduction to metallic iron and rutile, which was followed by a slow reduction of rutile to a series of oxides with the general formula Ti_nO_{2n-1} until Ti_3O_5 was formed, which was found to be relatively stable.

During the heating process of the composites of titanomagnetite concentrates and carbonaceous material, several reactions will occur, which include solid–solid reduction reactions by carbon, gas–solid reduction reactions with CO as the reductant, and the strongly endothermic gasification reaction between carbon and CO_2.[25–33] Due to its complexity, it is meaningful to understand the reduction behavior of Panzhihua titanomagnetite concentrate (PTC)-coal composites well. In the current study, reduction of composites of PTC and coal was investigated by thermogravimetric analysis and temperature-programmed heating experiments.

II. EXPERIMENTAL

A. *Raw Materials and Experimental Procedures*

Chemical compositions and size distribution of PTC and coal were examined and are presented in Tables I through III. Figure 1 shows the X-ray diffraction (XRD) pattern of PTC. The mineral compositions were majorly titanomagnetite and magnetite and ilmenite. The PTC was mixed homogenously with the coal. The molar ratio of $C_{fixed}/O_{(bonded\ with\ Fe)}$ in the mixture was fixed at 1.2 to ensure the complete reduction of iron-bearing oxides to metallic iron. The mixture was made as spheroidic briquette under the pressure of 15 MPa with a briquette maker. The diameter of the briquette was 30 mm and the total mass of the sample was about 20 g. All the briquettes were dried for 6 hours at 393 K (120 °C) before the reduction experiments. Table II.

The reduction behaviors of the briquettes were investigated by temperature-programmed heating in a vertical tube electric furnace, whose schematic is shown in Figure 2. There was a uniform temperature zone with about 120 mm height in the furnace tube, and the temperature was measured with an S-type thermocouple. A single briquette was used for each experiment. The furnace temperature was controlled with the programs in which the heating rate is 5 K (5 °C)/ min and there was a 30- minute holding time when the temperature reached 1173 K, 1273 K, 1473 K, and 1573 K (900 °C, 1000 °C, 1200 °C, and 1300 °C), respectively. Before heating, the furnace tube was first vacuumized with the valve 1 closed and valve 2 open. When the pressure inside the furnace tube measured with a pressure meter decreased to dozens of pascal, valve 2 was closed and the tube was backfilled

Table I. Chemical Composition of PTC and Coal, Weight Percentage

PTC								Coal			
TFe	FeO	TiO_2	V_2O_5	SiO_2	CaO	MgO	Al_2O_3	C	Volatile	Ash	S
52.62	32.0	12.0	0.6	4.2	1.3	2.6	3.9	81.95	6.95	10.41	0.69

Table II. Size Distribution of PTC

Diameter (μm)	<74	74 to 80	80 to 96	96 to 109	109 to 120	120 to 150	>150	Total
Content (wt pct)	88.40	3.26	4.20	1.86	1.81	0.32	0.15	100

Table III. Size distribution of coal

Diameter (μm)	<100	150 to 180	180 to 250	250 to 550	550 to 1700	>1700	Total
Content (wt pct)	20.80	51.34	14.81	9.87	2.00	1.18	100

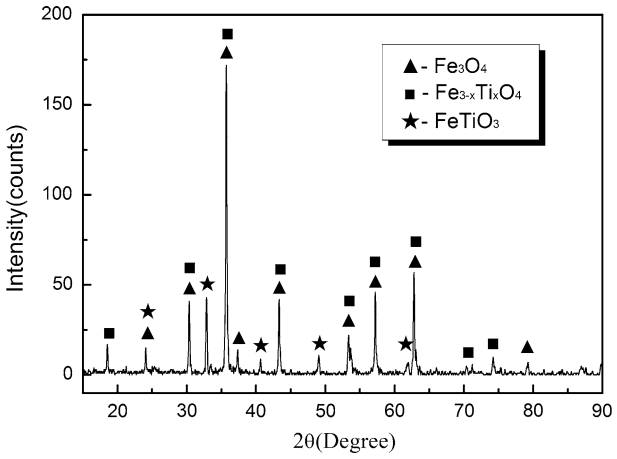

Fig. 1—XRD pattern of PTC.

with argon until the pressure inside returned to one atmospheric pressure. Then, valve 1 was opened and the flow rate of argon was kept at 0.5NL/ min. The compositions of off-gas from the furnace tube were continuously analyzed with an online infrared gas analyzer (Model # Gasboard-3100P; Wuhan Cubic Optoelectronics Co., Ltd., Wuhan, China) and the flow rate of that was continuously measured by a mass flow meter (Model # MF4008, standardized with argon; Siargo Ltd., Santa Clara, CA). Off-gas compositions and flow rate readings was taken two times a minute and directly logged onto a computer with a data-acquisition system. During the reduction experiments, the pressure in the furnace was kept close to one atmospheric pressure.

The mass loss behavior of the mixture was also checked with the TG (thermogravimetry) and DTG (derivative thermogravimetry) method, which was carried out in a NETZSCH STA 449C thermal analyzer (NETZSCH Pumps North America, LLC, Exton, PA). The heating rate is 5 K (5 °C)/ min in an argon atmosphere from room temperature to 1773 K (1500 °C). About 70 mg mixture was used for each experiment.

The phase transformation during reduction was investigated in the vertical tube electric furnace by heating the briquettes in argon with a heating rate of 20 K (20 °C)/ min from room temperature to the different desired temperatures and holding for 30 minutes. Then, the briquette was rapidly moved to the low-temperature zone in the lower part of the furnace, followed by quenching. The reduced briquettes were examined by XRD, which was conducted using a Cu K_α source.

B. *Calculation of Reduction Degree*

The reduction degree (R) can be calculated from the composition and flow rate of the outlet gas from the reaction tube according to Eq. [1], given as:

$$R = \frac{16 \int_0^t N_O dt}{M_O} \quad [1]$$

where M_O (g) is the total mass of removable oxygen from iron oxide to metallic iron in a single briquette in theory and N_O (mol/ min) is the mole generation rate of oxygen at reduction time t (min).

Due to the mass flow meter used to measure the off-gas flow rate is standardized with argon, the mass flow meter readings is unreal when a different gas is flowed through it. So, it is imperative to calibrate the mass flow meter by introducing a correction factor γ_i, which can be obtained from Eq. [2]:

$$\gamma_i = \frac{F_i^M}{F_i^R} \quad [2]$$

where F_i^M (NL/ min) is the measured flow rate for gaseous species i obtained from the mass flow meter used to measure the off-gas flow rate during the reduction experiment and F_i^R (NL/ min) is the real flow rate for gaseous species i.

Calibrations of γ_i for the primary gaseous species (CO, CO_2, and CH_4) generated during the reduction process were performed. In a typical calibration, the gas was first flowed through a standard mass flow meter for gaseous species i at a certain flow rate (F_i^R) before flowed into furnace tube, which was purified previously with the gas for calibration. The outlet gas flow rate (F_i^M) was measured using the mass flow meter used to measure the off-gas flow rate during the reduction experiment and the readings were recorded until stabilization of the readings. Three calibrations were carried out for each gaseous species by fixing F_i^R at 0.5, 1.0, and 1.5 NL/ min, respectively, and the average was used in the calculation of reduction degree. In the current study, the value of γ_{CO}, γ_{CO_2}, and γ_{CH_4} were calibrated to approximately 1.02, 0.75, and 1.18, respectively. The correction factor (γ_{Ar}) for argon is equal to 1.

At a reduction time t, the measured off-gas flow rate can be represented as follows:

$$F_{og}^M = \sum F_i^M = \sum \gamma_i F_i^R \quad [3]$$

where F_{og}^M (NL/ min) is the measured off-gas flow rate. Moreover, F_i^R can be expressed by the following expression:

$$F_i^R = F_{og}^R \cdot x_i \quad [4]$$

where F_{og}^R (NL/ min) represents the real off-gas flow rate and x_i is the volume fractions for gaseous species i in off-gas, which were obtained from the infrared gas analyzer.

Thus, F_{og}^M can be represented by the following equation:

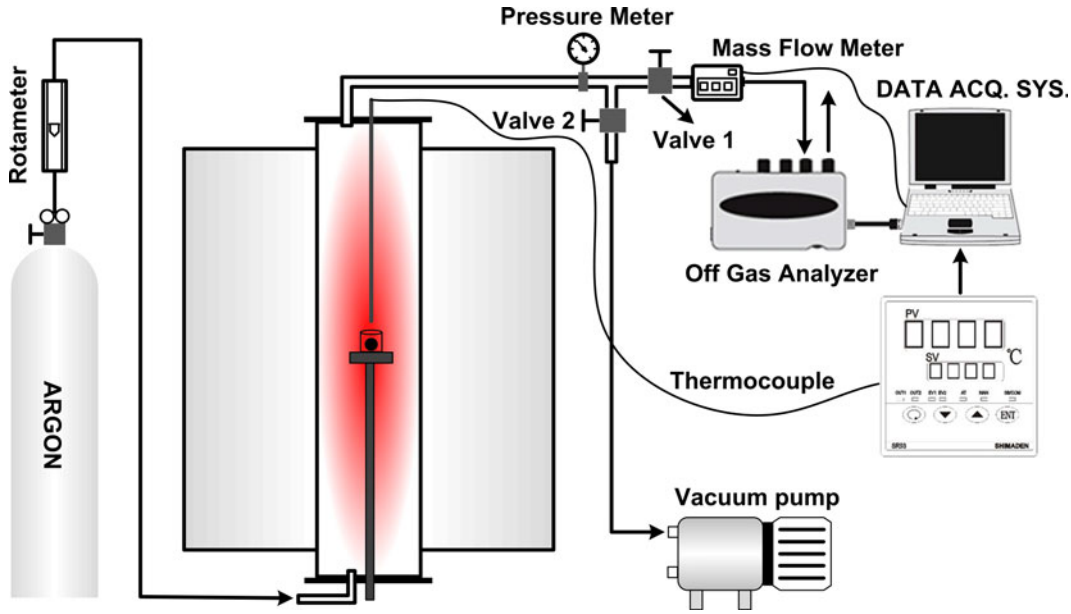

Fig. 2—Schematic of experimental system.

$$F_{\text{og}}^{M} = F_{\text{og}}^{R} \sum \gamma_i x_i \quad [5]$$

The mole generation rate of oxygen at reduction time t can be calculated according to the following expression:

$$N_{\text{O}} = \frac{F_{\text{og}}^{R}}{22.4}(x_{\text{CO}} + 2x_{\text{CO}_2}) = \frac{F_{\text{og}}^{M}}{22.4}\left(\frac{x_{\text{CO}} + 2x_{\text{CO}_2}}{\gamma_{\text{CO}} x_{\text{CO}} + \gamma_{\text{CO}_2} x_{\text{CO}_2} + \gamma_{\text{CH}_4} x_{\text{CH}_4} + \gamma_{\text{Ar}} x_{\text{Ar}}}\right) \quad [6]$$

So, Eq. [1] can be rewritten as:

$$R = \frac{16 \int_0^t \frac{F_{\text{og}}^{M}}{22.4}\left(\frac{x_{\text{CO}}+2x_{\text{CO}_2}}{\gamma_{\text{CO}} x_{\text{CO}}+\gamma_{\text{CO}_2} x_{\text{CO}_2}+\gamma_{\text{CH}_4} x_{\text{CH}_4}+\gamma_{\text{Ar}} x_{\text{Ar}}}\right) dt}{M_{\text{O}}} \quad [7]$$

III. THERMODYNAMIC CALCULATION

It is now generally accepted that the mechanism of carbothermic reduction of iron oxides is two-stage mechanism with the participation of gaseous intermediate (CO and CO_2) according to the following equations[30,32,34,35]:

$$\text{Fe}_x\text{O}_y + \text{CO} = \text{Fe}_x\text{O}_{y-1} + \text{CO}_2 \quad [8]$$

$$\text{CO}_2 + \text{C} = 2\text{CO} \quad [9]$$

Figure 3 shows the equilibrium atmosphere for main reactions occurring in the reduction of titanomagnetite concentrates, the data of which were calculated using the FactSage thermodynamics software package (Thermfact Ltd.-CRCT, Montréal, Canada[36]). It indicates that titanium-bearing iron oxides are more difficult to reduce than iron oxides by CO because higher $P_{\text{CO}}/(P_{\text{CO}} + P_{\text{CO}_2})$ is required for the reductions of titanium-bearing iron oxides.

A stepwise reduction of ilmenite was found from the calculation, which is also a "fork-like" reduction mechanism. The critical temperature is 1423 K (1150 °C), lower than the temperature at which the ilmenite ($FeTiO_3$) is reduced to iron and rutile, and higher than the temperature at which the reduction of ilmenite becomes stepwise with ferrous-pseudobrookite ($FeTi_2O_5$) as the intermediate phase. This is because of the instability of ferrous-pseudobrookite at temperatures lower than 1423 K (1150 °C) according to the equilibrium binary phase diagram of FeO-TiO_2 (Figure 4), which was calculated using the FactSage thermodynamics software package. Thermodynamically, the rutile can be reduced to lower valence oxides in a CO/CO_2 atmosphere when the temperature is higher than 1373 K (1100 °C).

IV. RESULTS AND DISCUSSION

A. *Reduction Behavior of PTC-Coal Composites*

The TG and DTG curves of PTC-coal mixture in argon are shown in Figure 5. It is indicated that the mass loss of mixture started from 743 K (470 °C) and finished at approximately 1703 K (1430 °C). There are four apparent peaks found in the DTG curve, revealing the evolution of reaction rate of mixture during the heating process, from which five stages of mass loss can be found.

In the first stage (743 K to 1003 K [470 °C to 730 °C]), due to the release of the volatiles in the coal at this temperature range, there was a little mass loss.

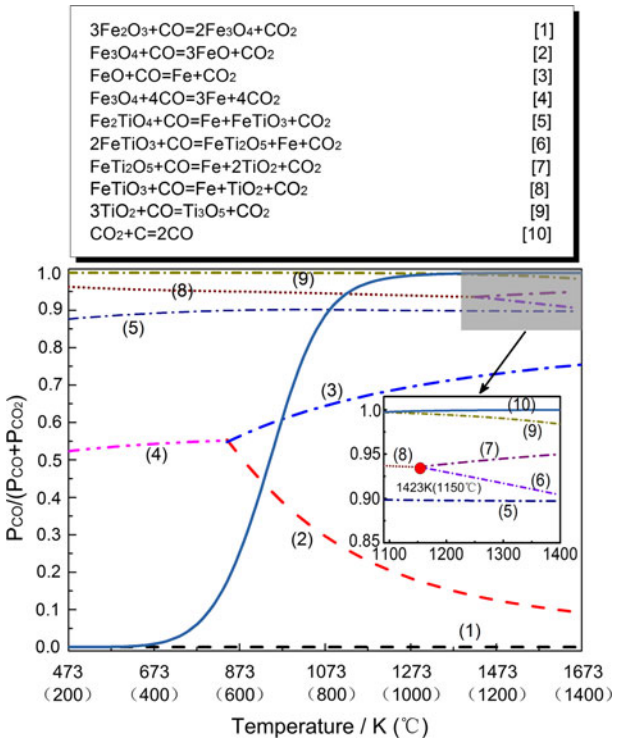

Fig. 3—Dependency of equilibrium atmosphere for reactions mainly occurred in the reduction of titanomagnetite concentrates on temperature. (Data from FToxid-FACT oxide database 2010.).

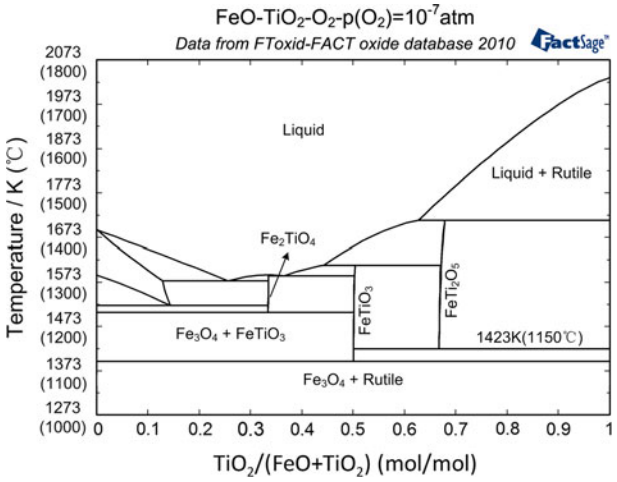

Fig. 4—FeO-TiO_2 phase diagram.

In the second stage (1003 K to 1233 K [730 °C to 960 °C]), the mass loss rate represented in DTG curve increased quickly from 1003 K (730 °C) and reached the maximum at 1193 K (920 °C) followed with a short plateaus, but the mass loss was still little from the TG curve. It indicates that the reduction rate is relatively slower due to the slow carbon gasification rate in this stage. It has been established that reduction rate of iron oxide-coal composites is controlled by the gasification reaction rate at temperatures lower than 1273 K (1000 °C).[13–15,37]

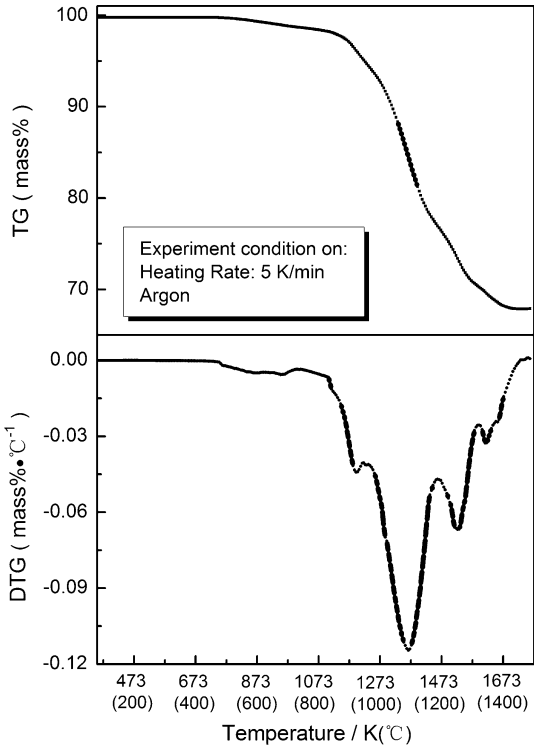

Fig. 5—TG and DTG curves for linear heating reduction of PTC-coal mixture.

During the third stage (1233 K to 1463 K [960 °C to 1190 °C]), the mass loss increased dramatically as revealed in the TG curve, and the mass loss rate increased dramatically and up to the maximum in the whole heating process and then decreased with the heating going. It is suggested that the reduction rate became fast in this stage. It is substantiated that the rate of carbon gasification become significant when temperature is higher than 1273 K (1000 °C), resulting in the acceleration of reduction rate.[13,14,38]

At the fourth stage (1463 K to 1593 K [1190 °C to 1320 °C]), when the sample was heated to about 1463 K (1190 °C), the mass loss rate began to increase again and then decreased after it was heated to about 1523 K (1250 °C). According to Figure 3, ilmenite is more thermodynamically difficult to be reduced than that of iron oxides due to the higher requirement for the $P_{CO}/(P_{CO}+P_{CO_2})$ ratio. Thus, reduction reactions, mainly the reduction of ilmenite ($FeTiO_3$), probably occurred at this stage.

During the fifth stage (>1593 K [1320 °C]), there was a relatively small mass loss compared to that at the fourth stage. It is suggested that a reduction of titanium oxides, which were available at a high temperature, probably occurred in this period.

Figure 6 shows the composition of off-gas generated during reduction of PTC-coal briquette. It was observed that the generation rate of gaseous species, indirectly representing the reduction rate, changed during the heating process. When the temperature reached about 753 K (480 °C), the methane began to generate and almost finished until 1013 K (740 °C), which can be

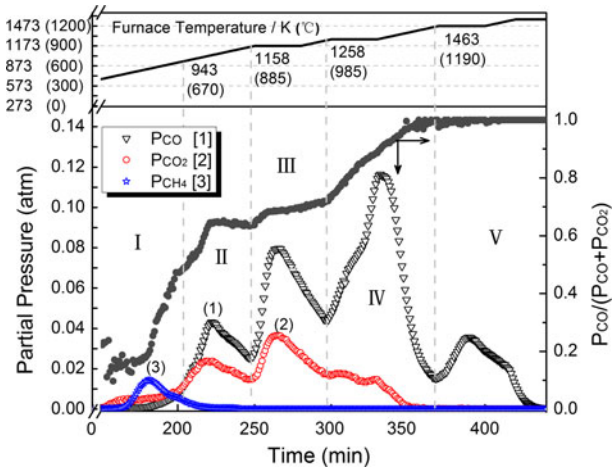

Fig. 6—Temperature regime and partial pressure profiles of primary gaseous species generated during the reduction of coal-mixed PTC briquette.

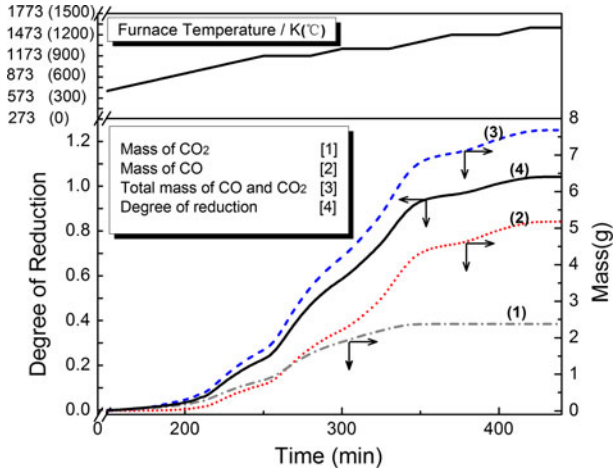

Fig. 7—Total mass with respective amounts of CO and CO_2 generated and degree of reduction with time.

attributed to the devolatilization of coal. It can be seen that, at the initial stage, there was little CO generated, and the partial pressure of CO_2 was higher than that of CO. The greater amount of CO started to generate at 823 K (550 °C), and its concentration quickly exceeded CO_2 at about 943 K (670 °C). In the following two stages, the evolution behavior of CO_2 was similar to that of CO, which increased first and then decreased and backed to rise again, although the generation rate differed from that of CO. The $P_{CO}/(P_{CO} + P_{CO_2})$ ratio shown in Figure 6 increased rapidly and got to a plateaus, with a $P_{CO}/(P_{CO} + P_{CO_2})$ ratio of 0.64 at about 1023 K (750 °C). When the temperature remained at 1173 K (900 °C), the $P_{CO}/(P_{CO} + P_{CO_2})$ ratio ascended followed by a plateau and then increased slowly to 0.72 at 1258 K (985 °C). The equilibrium $P_{CO}/(P_{CO} + P_{CO_2})$ ratio for the FeO→Fe reduction varies from 0.54 to 0.69 if the temperature varies from 843 K to 1273 K (570 °C to 1000 °C), as shown in Figure 3. Therefore, it indicated that the iron oxides reduction, especially reduction of wustite to metallic iron, mainly occurred in the second and third stages. In the fourth stage, the CO partial pressure reached the maximum in the whole heating process and then decreased, while the CO_2 partial pressure began to drop gradually from the third stage. This is because of the drastic carbon gasification reaction by CO_2 at temperature over 1273 K (1000 °C). It is suggested that the reduction of ilmenite ($FeTiO_3$) are the main reaction occurred in the fourth stage. Only CO was detected in the final stage, the reduction of ferrous-pseudobrookite ($FeTi_2O_5$) is considered as the main reaction and rutile is probably reduced in the stage, which is confirmed by the XRD analysis and will be discussed below.

Figure 7 shows the mass change of CO and CO_2 obtained from gas analysis and the degree of reduction as a function of heating time during the temperature-programmed heating. It shows that the final degree of reduction (R) slightly exceeds 1. This might be the reason that a small amount of titanium oxides was reduced to their lower valence oxides involving the generation of CO and CO_2.

B. *Phase Transformation of Composite Briquettes Reduced at Different Temperatures*

The briquettes were heated at different temperatures for 30 minutes, and the phase transformations of the PTC were investigated by XRD, the patterns of which are shown in Figure 8. The main phases of sample reduced at 1173 K (900 °C) are metallic iron, ilmenite ($FeTiO_3$), and titanomagnetite ($Fe_{3-x}Ti_xO_4$). The traces of rutile (TiO_2) were observed in the sample at 1273 K (1000 °C). Iron carbide (Fe_3C) and ferrous-pseudobrookite [$(Fe,Mg)Ti_2O_5$], in which some Fe^{2+} was replaced by Mg^{2+}, appeared in the sample reduced at 1473 K (1200 °C). Traces of $MgTiO_3$ were detected in the XRD pattern of a sample heated up to 1573 K (1300 °C). Ferrous-pseudobrookite disappeared and titanium carbide (TiC) was observed in the sample at 1623 K (1350 °C).

Based on the XRD analysis, the reduction path of PTC briquette with coal under the experimental condition is shown schematically in Figure 9. The following reduction sequence can be suggested:

$$Fe_3O_4 \rightarrow Fe \qquad [10]$$

$$Fe_{3-x}Ti_xO_4 \rightarrow FeTiO_3 + Fe \qquad [11]$$

$$FeTiO_3 \rightarrow TiO_2 + Fe \ (< 1423 \text{ K } [1150°C]) \qquad [12a]$$

$$FeTiO_3 \rightarrow FeTi_2O_5 + Fe \rightarrow TiO_2 + Fe \ (\geq 1423 \text{ K } [1150°C]) \qquad [12b]$$

It is noticed that wustite (FeO) and ulvospinel (Fe_2TiO_4), which exist in the equilibrium reduction path[5,39,40] as intermediate phases, were not detected by

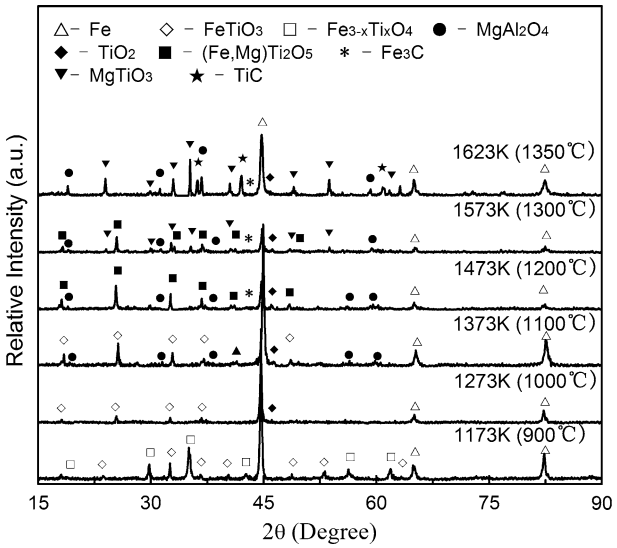

Fig. 8—XRD patterns of coal-mixed PTC briquettes reduced at different temperatures after 30 min.

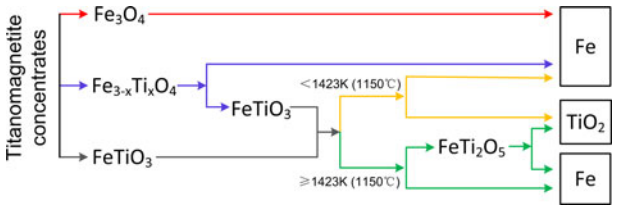

Fig. 9—Phase transitions of coal-mixed PTC briquettes reduced at different temperatures for 30 min.

XRD in these experiments. This is because the wustite (FeO) and ulvospinel (Fe_2TiO_4) formed in the process of composite briquette reduction were quickly reduced to metallic iron and ilmenite,[4,5] and the 30 minutes holding time when temperature reached the preset values could be responsible.

C. *Shrinkage of Reduced Briquettes and Nucleation of Reduced Iron Particles*

The shrinkage of reduced briquettes *Sh* was calculated by Eq. [13], given as follows[36]:

$$Sh = \frac{D_r}{D_i} \times 100\,\text{pct} \qquad [13]$$

where D_i and D_r are the diameter of initial briquette and the reduced briquette at certain temperature for 30 minutes, respectively. The diameter of each briquette was measured many times from different diametrical direction for each sample. The average value of the diameter was obtained and the result is shown in Figure 10.

It is revealed that the shrinkage of briquettes depended on temperature greatly. At a higher temperature, the larger shrinkage was observed, which could be attributed to greater removal of carbon and oxygen from the briquette by reactions and the particles get denser by a sintering mechanism by increasing the temperature. It shows that shrinkage increased abruptly at a temperature higher than 1473 K (1200 °C). This is primarily because the reduced iron migrates from the inside to the outside of a briquette to form a nugget. As shown in Figure 11, the iron nugget was observed at the surface of briquette. This could be attributed to the formation of iron carbides by the carburization reaction between iron formed by reduction and excess carbon, which was added for ensuring the complete reduction of iron-bearing oxides, in the briquette at a higher temperature. For a higher temperature, the greater shrinkage leads to the more intimate contact between reduced iron and excess carbon, which facilitates the kinetics of the carburization reaction. The carbon contents of iron nuggets were examined by the high-frequency combustion-infrared absorption spectrometric method, which are 1.39 pct and 1.51 pct for briquettes reduced at 1573 K and 1623 K (1300 °C and 1350 °C), respectively. Figure 12 is the equilibrium phase diagram of the Fe-C system. It is revealed that the onset of liquid phase appearance at 1556 K (1283 °C) for the carbon content of 1.39 pct in the iron nugget and 1537 K (1264 °C) for that of 1.51 pct. This means that liquid metal is formed during the reduction at 1573 K and 1623 K (1300 °C and 1350 °C). Therefore, due to the carburization, the reduced iron can migrate to form a nugget by driving the capillary force from the inside to the outside of the briquette, resulting from minimizing the surface energy at 1573 K and 1623 K (1300 °C and 1350 °C) under the current experimental conditions.

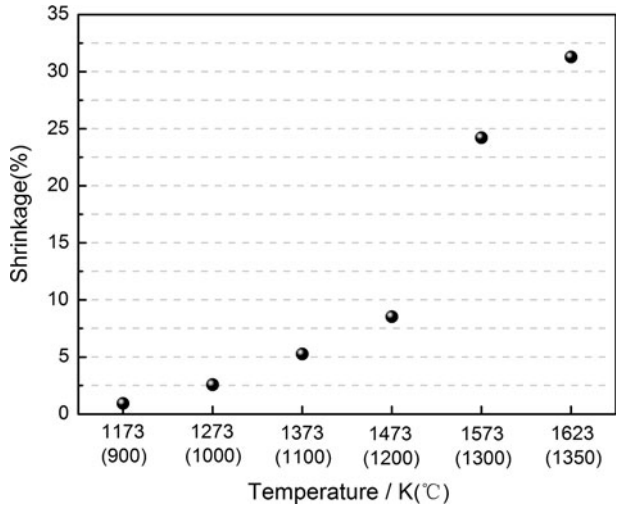

Fig. 10—Shrinkage of coal-mixed PTC briquettes reduced at different temperature after 30 min.

V. CONCLUSIONS

The temperature-programmed heating of the PTC-coal mixture and coal-mixed PTC briquette in argon were carried out to investigate the carbothermic reduction behavior of the PTC. The following conclusions were obtained:

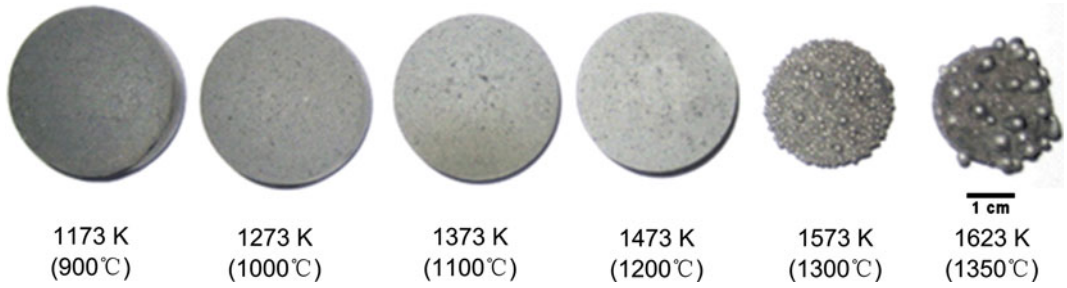

Fig. 11—Overall view of reduced coal-mixed PTC briquettes.

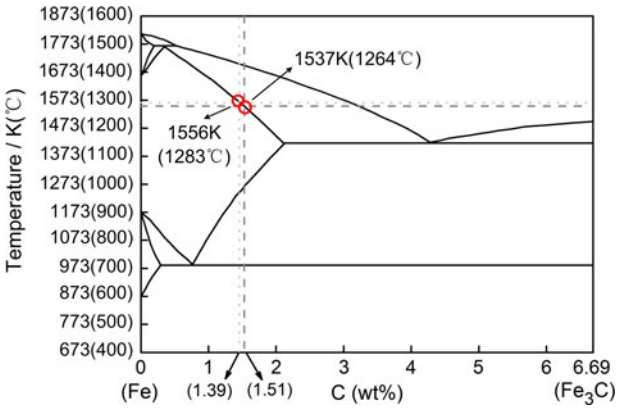

Fig. 12—Phase diagram of the iron-carbon system.

1. Five stages were found in the carbothermic reduction of PTC briquette with coal. The devolatilization of coal occurred in the first stage, and reductions of iron oxides occurred mainly in the second and third stages. The reduction rate of iron oxide in the third stage was much higher than that in the second stage because of the high carbon gasification rate. The iron in the ilmenite ($FeTiO_3$) was reduced in the fourth stage. In the final stage, TiO_2 was partially reduced to lower valence oxides.
2. The phase transformation of the briquettes are shown in Figure 9. The main phases of sample reduced at 1173 K (900 °C) are metallic iron, ilmenite ($FeTiO_3$), and titanomagnetite ($Fe_{3-x}Ti_xO_4$). The traces of rutile (TiO_2) were observed at 1273 K (1000 °C). The iron carbide (Fe_3C) and ferrous-pseudobrookite ($FeTi_2O_5$) appeared at 1473 K (1200 °C). The titanium carbide was found in the sample reduced at 1623 K (1350 °C). Wustite (FeO) and ulvospinel (Fe_2TiO_4) were not found in the current study.
3. Shrinkages of reduced briquettes were found to depend on the temperature greatly; the briquette gets denser with an increase in the temperature. Nuggets were observed outside of briquette reduced at 1573 K (1300 °C) and a higher temperature. The nugget formation can indicate a new process of ironmaking with titanomagnetite similar to ITmk3 (Ironmaking Technology Mark 3).[41,42]

ACKNOWLEDGMENTS

The authors are especially grateful to Major Program of National Natural Science Foundation of China (Grant No. 51090383 and No. 51090382), and also to Scholarship Award for Excellent Doctoral Student granted by Ministry of Education (Grant No. 0903005109081-8).

REFERENCES

1. D. Chen, B. Song, L.N Wang, T. Qi, Y. Wang, and W.J. Wang: *Miner. Eng.*, 2011, vol. 24 (8), pp. 864–69.
2. J.S. Zhu: *Min Metall. Eng*, 1997, vol. 17 (1), pp. 20–24.
3. Panzhihua Resource Comprehensive Utilization Office: 1985, vol. 16 (1), pp. 6–19, 243–54.
4. E. Park and O. Ostrovski: *ISIJ Int.*, 2003, vol. 43 (9), pp. 1316–25.
5. E. Park and O. Ostrovski: *ISIJ Int.*, 2004, vol. 44 (6), pp. 999–1005.
6. C.I. Pearce: Lawrence Berkeley National Laboratory, 2010.
7. Panzhihua Resource Comprehensive Utilization Office: 1985, vol. 6 (2), pp. 453–67.
8. Panzhihua Resource Comprehensive Utilization Office: 1985, vol. 6 (3), pp. 509–18, 700–37, 793–829.
9. L.H. Zhou, D.P. Tao, M.X. Fang, F.H. Zeng, and X. Pu: *Chin. J. Rare Met.*, 2009, vol. 33 (3), pp. 406–10.
10. S.Q. Kang: *Sintering Pelletizing*, 1989, vol. 4, pp. 15–19.
11. X. Xue: *Iron Steel Vanadium Titanium*, 2007, vol. 28 (3), pp. 37–41.
12. V.E. Roshchin, A.V. Asanov, and A.V. Roshchin: *Russ. Metall. (Metally)*, 2010, vol. 11, pp. 1001–08.
13. R.J. Fruehan: *Metall. Trans. B*, 1977, vol. 8B, pp. 279–86.
14. K. Otsuka and D. Kunii: *J. Chem. Eng. Jpn.*, 1969, vol. 2, pp. 46–50.
15. Y.K. Rao: *Chem. Eng. Sci.*, 1974, vol. 29, pp. 1435–45.
16. N.S. Srinivasan and A.K. Lahiri: *Metall. Trans. B*, 1977, vol. 8B, pp. 175–78.
17. C. Bryk and W.K. Lu: *Ironmaking Steelmaking*, 1986, vol. 13, pp. 70–75.
18. B.H. Huang and W.K. Lu: *ISIJ Int.*, 1993, vol. 33 (10), pp. 1056–61.
19. C.E. Seaton, J.S. Foster, and J. Velasco: *Trans. Iron Steel Inst. Jpn.*, 1983, vol. 23, pp. 490–96.
20. S. Sun and W.K. Lu: *ISIJ Int.*, 1993, vol. 33 (10), pp. 1062–69.
21. M.A.R. Dewan, G. Zhang, and O. Ostrovski: *ISIJ Int.*, 2010, vol. 50 (5), pp. 647–53.
22. S.K. Gupta, V. Rajakumar, and P. Grieveson: *Metall. Trans. B*, 1987, vol. 18B, pp. 713–18.
23. S.K. Gupta, V. Rajakumar, and P. Grieveson: *Metall. Trans. B*, 1989, vol. 20B, pp. 735–45.
24. N.J. Welham and J.S. Williams: *Metall. Mater. Trans. B*, 1999, vol. 30B, pp. 1075–81.
25. R.J. Longbottom, O. Ostrovski, and E. Park: *ISIJ Int*, 2006, vol. 46 (5), pp. 641–46.
26. B.V. L'vov: *Thermochim. Acta*, 2000, vol. 360, pp. 109–20.
27. K. Ishizaki, K. Nagata, and T. Hayashi: *ISIJ Int.*, 2006, vol. 46 (10), pp. 1403–09.

28. N.J. Welham and J.S. Williams: *Metall. Mater. Trans. B*, 1999, vol. 30B, pp. 1075–81.
29. R.H. Tien and E.T. Turkdogan: *Metall. Trans. B*, 1977, vol. 8B, pp. 305–13.
30. D. Chakraborty, S. Ranganathan, and S.N. Sinha: *Metall. Mater. Trans. B*, 2009, vol. 41B, pp. 10–18.
31. M.A.R. Dewan, G. Zhang, and O. Ostrovski: *Metall. Mater. Trans. B*, 2009, vol. 41B, pp. 182–92.
32. O.M. Fortini and R.J. Fruehan: *Metall. Mater. Trans. B*, 2005, vol. 36B, pp. 865–72.
33. S. Halder and R.J. Fruehan: *Metall. Mater. Trans. B*, 2008, vol. 39B, pp. 784–95.
34. P.N. Ostrik and A.N. Popov: *Powder Metall. Met. Ceram.*, 1974, vol. 13 (5), pp. 371–76.
35. R.H. Tien and E.T. Turkdogan: *Metall. Trans. B*, 1977, vol. 8B, pp. 305–13.
36. S. Halder and R.J. Fruehan: *Metall. Mater. Trans. B*, 2008, vol. 39B, pp. 809–17.
37. M.C. Abraham and A. Ghosh: *Ironmaking Steelmaking*, 1979, vol. 6, pp. 14–23.
38. S.K. Dutta and A. Ghosh: *Metall. Mater. Trans. B*, 1994, vol. 25B, pp. 15–26.
39. A.F. Buddington and D.H. Lindsley: *J. Petrology*, 1964, vol. 5 (2), pp. 310–57.
40. G.D. McAdams: *Ironmaking Steelmaking*, 1974, vol. 1, p. 138.
41. T. Harada and H. Tanaka: *ISIJ Int.*, 2011, vol. 51 (8), pp. 1301–07.
42. H. Ishikawa, J. Kopfle, J. Mcclelland, and J. Ripke: *Arch. Metall. Mater.*, 2008, vol. 53 (2), pp. 541–45.